ARTICLE IN PRESS

Computers and Mathematics with Applications ▮ (▮▮▮▮) ▮▮▮–▮▮▮

Contents lists available at ScienceDirect

Computers and Mathematics with Applications

journal homepage: www.elsevier.com/locate/camwa

A simple phase-field model for interface tracking in three dimensions

Abbas Fakhari [a,*], Martin Geier [b], Diogo Bolster [a]

[a] Department of Civil and Environmental Engineering and Earth Sciences, University of Notre Dame, Notre Dame, IN 46556, USA

[b] TU Braunschweig, Institute for Computational Modeling in Civil Engineering (iRMB), TU-Braunschweig, Pockelsstr. 3, 38106 Braunschweig, Germany

ARTICLE INFO

Article history:
Available online xxxx

Keywords:
Conservative phase-field
Three-phase contact line
Interface tracking
Diffuse-interface modeling
Contact angle
Lattice Boltzmann method

ABSTRACT

Based on a conservative phase-field lattice Boltzmann (LB) method, we present a 3D model for tracking an interface in multiphase flows. In addition to being mass-conserving, the main advantage of this LB method is that the collision process is made entirely local by invoking central moments in the calculation of vectors normal to the interface. We construct the model on different 3D lattices (D3Q7 and D3Q15) with inherently distinct isotropy properties. To test the model we conduct a variety of benchmark studies, such as the evolution of an interface in the form of a slotted sphere in a rotational flow field, and the evolution of a spherical interface in a vortex flow, a deformation flow, and a shear flow. The results of these benchmarks are compared against the finite-difference-based version of the LB model, in which a non-local finite-difference scheme is used to calculate the interface normal. In terms of error, the moment-based model, while competitive, is generally outperformed by the finite-difference model. Despite this, the moment-based interface tracking model is inherently more efficient, and deserves consideration, particularly for memory-distributed parallel computing. We also consider the interaction between a binary fluid and a solid wall, and introduce a method to implement the three-phase contact angle within this framework. The proposed model for dealing with the contact line is simple, clean, and straightforward to implement, and shown to recover desired contact angles very well.

1. Introduction

Interface tracking equations and their application are an indispensable part of multiphase flow solvers in modern computational fluid dynamics. Across the literature there are many numerical schemes for tracking interfaces between different fluids [1], which, among others, include the volume-of-fluid method [2], front-tracking techniques [3,4], and level set methods [5,6]. Phase-field approaches are another class of models that have attracted attention in this area [7,8]. The primary difference between this approach and others is that instead of solving a pure advection equation, an advection–diffusion-type equation is solved to represent the interface within a diffuse interface context.

To date, the majority of phase-field interface-tracking models invoke Cahn–Hilliard (CH) theory [9]. The CH equation is derived by minimizing a free-energy functional. The interface evolution is then governed by the difference in chemical potential of the fluids. This chemical potential, which is typically obtained by considering a double-well potential barrier and curvature effects, tends to zero at thermodynamic equilibrium. If the system is pushed out of its equilibrium state, the

* Corresponding author.
E-mail address: afakhari@nd.edu (A. Fakhari).

http://dx.doi.org/10.1016/j.camwa.2016.08.021
0898-1221/

Please cite this article in press as: A. Fakhari, et al., A simple phase-field model for interface tracking in three dimensions, Computers and Mathematics with Applications (2016), http://dx.doi.org/10.1016/j.camwa.2016.08.021

chemical potential creates a force imbalance in such a way as to minimize the free energy of the system. The Allen–Cahn equation [10], which is particularly useful in the study of solidification processes, is a related approach for tracking the phase-field variable. Motivated by this approach, Sun and Beckermann [11] proposed a simpler phase-field model for tracking the interface between two fluids, which was later reformulated in conservative form [12]. In this model, the phase field evolves by considering the balance between advective, diffusive, and phase-separation fluxes across the fluid interface. We refer to this scheme as the conservative phase-field (CPF) model.

While both aim to represent similar behaviors, there are some key differences between the CH and CPF equations. Mathematically, the CH equation includes spatial derivative terms of second and fourth order. Numerically, this can be disadvantageous; not only does this diminish the locality of a numerical scheme, but also there is a reduction in numerical accuracy due to the need to calculate the Laplacian (∇^2) of another term, which itself includes the calculation of a Laplacian within in [13]. The CPF equation, on the other hand, is driven by curvature and only requires the calculation of first-order and second-order derivatives, much more ideal for efficient numerical implementation. Even the more troublesome second-order derivative can be further reduced to calculation of only first-order derivatives within the framework of Lattice Boltzmann Methods (LBM) [14].

LBM is a class of mesoscopic approaches developed for the solution of a variety of partial differential equations, including the advection–diffusion and Navier–Stokes equations [15–18]. Lattice Boltzmann Equations (LBEs) are derived by considering spatial and temporal changes in a Maxwellian particle distribution function [19]. Specifically, LBEs are solved by partitioning the movement of particles into two steps: collision and advection. On commonly used structured uniform grids, the solution to the advection step is a perfect shift, which is also known as *streaming*. During the collision process, the discrete distribution function is updated to account for interactions between particles. One of the interesting features of the LBE, in the absence of external forces, is that all the nonlinearity in the governing equations is local (collision) and all the nonlocality is linear (streaming). This property is extremely useful and makes LBM highly scalable in terms of parallel computing. However when an external force, such as interfacial tension, is present this powerful feature can be lost. This is the case for multiphase systems where typically one must compute features such as the curvature or the normal vector to the interface, among other factors.

Although there have been partial attempts to develop an LBE with an entirely local collision step for tracking the interface between different fluids [20,21], the majority of interface tracking LB models are best described as hybrid finite-difference (FD) LBM [13,22–26]. Until recently [14], all previous interface tracking LB models, based on CH theory, appeal to finite-differences for calculating the gradients required for computation of the curvature or interface normal. Using FD schemes not only reduces the efficiency of cache-based computers, but also compromises the locality of the LBM.

Another important multiphase system that prior CPF based studies have not considered is the problem of a three-phase contact line. Although methods based on CH theory are available for treatment of the contact angle between a binary fluid and a solid wall [27], little to no work has been done in dealing with arbitrary contact angles using CPF models. This is mainly due to the fact that CPF models are relatively new [12], particularly within the LBE framework [14]. Given the importance of fluid–solid interactions in natural and engineering applications (*e.g.*, multiphase flow through porous media [18]), modeling the triple fluid–fluid–solid contact line is a crucial problem that must be addressed. In this study we aim to fill this gap.

Recently, we proposed a clean LBM for tracking the interface between two different phases in 2D [14]. By clean we mean that the collision step was constructed to be purely local. Knowing that LBM inherently recovers conservation laws in their conservative form, we develop a three-dimensional LBM to mimic the CPF equation. We use central moments to formulate an LBE with an entirely local, and sufficiently accurate, collision step for both highly isotropic (D3Q15, D3Q19, and D3Q27) lattices and a minimally isotropic (D3Q7) lattice. We also formulate a supplemental FD-LBM, where finite-differences are used to calculate the required gradients, for interface tracking in 3D. Herein we call the former approach the moment-based LBM (*MB-LBM*) and the latter one the *FD-LBM*. The accuracy of the models is compared by applying them to four important benchmark problems. Finally, we propose an efficient and straightforward formula for treating a three-phase contact angle for fluid–solid interactions in both 2D and 3D systems.

2. Conservative phase-field LBE

For the sake of simplicity and brevity, herein we formulate the CFP equation using a single-relaxation-time (SRT) collision model. Generalizing this approach to the multi-relaxation-time (MRT) model or the cumulant approach should be straightforward [14,28]. We construct the model for the D3Q15 lattice as well as D3Q7. Compared with the D3Q7 lattice, the D3Q15 lattice is more isotropic, and therefore more accurate, and has better Galilean invariance properties. On the other hand, the D3Q7 is more efficient and requires less computational resources. Formulation of the model using higher-order (D3Q19 or D3Q27) lattices is also presented (see Appendix) but not implemented in this work.

Let us introduce the phase-field variable ϕ, which is used to identify different fluids within a multiphase system. For the binary fluid system considered here, $\phi = 1$ identifies phase 1 and $\phi = 0$ represents phase 2. The following conservative equation governs topological changes in the phase field [11,12]:

$$\frac{\partial \phi}{\partial t} + \nabla \cdot (\phi \mathbf{u}) = \nabla \cdot \left[M \left(\nabla \phi - \frac{4\phi(1-\phi)}{\xi} \mathbf{n} \right) \right] \tag{1}$$

Please cite this article in press as: A. Fakhari, et al., A simple phase-field model for interface tracking in three dimensions, Computers and Mathematics with Applications (2016), http://dx.doi.org/10.1016/j.camwa.2016.08.021

where t stands for time, $\mathbf{u}$ is the macroscopic velocity vector, M is the mobility, ξ is the interface thickness, and $\mathbf{n}$ is the unit vector normal to the interface defined by

$$\mathbf{n} = \frac{\nabla\phi}{|\nabla\phi|}. \tag{2}$$

The equilibrium phase-field profile for an interface located at $\mathbf{x} = \mathbf{x}_0$ is

$$\phi(\mathbf{x}) = \frac{1}{2}\left[1 - \tanh\left(\frac{2|\mathbf{x} - \mathbf{x}_0|}{\xi}\right)\right]. \tag{3}$$

In our previous work, we proposed the following LBE [14], which recovers Eq. (1):

$$h_\alpha(\mathbf{x} + \mathbf{e}_\alpha\delta t,\ t + \delta t) = h_\alpha(\mathbf{x},\ t) - \frac{h_\alpha(\mathbf{x},\ t) - h_\alpha^{eq}(\mathbf{x},\ t)}{\tau_\phi + 1/2} \tag{4}$$

where h_α is the phase-field distribution function, τ_ϕ is the relaxation time, and the equilibrium distribution function is given by

$$h_\alpha^{eq} = \phi\Gamma_\alpha + w_\alpha\frac{M}{c_s^2}\left[\frac{4\phi(1-\phi)}{\xi}\right](\mathbf{e}_\alpha \cdot \mathbf{n}) \tag{5}$$

where c_s is the lattice speed of sound, to be specified, and the relaxation time is related to the mobility by

$$M = \tau_\phi c_s^2 \delta t. \tag{6}$$

For the D3Q15 lattice the microscopic velocity set $\mathbf{e}_\alpha$ and the weight coefficients w_α are

$$\mathbf{e}_\alpha = c\begin{cases}(0,\ 0,\ 0), & \alpha = 0\\ (\pm1,\ 0,\ 0),\ (0,\ \pm1,\ 0),\ (0,\ 0,\ \pm1), & \alpha = 1-6\\ (\pm1,\ \pm1,\ \pm1), & \alpha = 7-14\end{cases} \tag{7}$$

and

$$w_\alpha = \frac{1}{72}\begin{cases}16, & \alpha = 0\\ 8, & \alpha = 1-6\\ 1, & \alpha = 7-14\end{cases} \tag{8}$$

and the dimensionless distribution function Γ_α is

$$\Gamma_\alpha = w_\alpha\left[1 + \frac{\mathbf{e}_\alpha \cdot \mathbf{u}}{c_s^2} + \frac{(\mathbf{e}_\alpha \cdot \mathbf{u})^2}{2c_s^4} - \frac{\mathbf{u}\cdot\mathbf{u}}{2c_s^2}\right] \tag{9}$$

where $c = \delta x/\delta t$ is the constant lattice speed and the speed of sound in Eqs. (5), (6), and (9) is $c_s = c/\sqrt{3}$. The microscopic velocities and weight coefficients for D3Q19 and D3Q27 are also provided in the Appendix.

For the D3Q7 lattice the microscopic velocity set and the weight coefficients are

$$\mathbf{e}_\alpha = c\begin{cases}(0,\ 0,\ 0), & \alpha = 0\\ (\pm1,\ 0,\ 0),\ (0,\ \pm1,\ 0),\ (0,\ 0,\ \pm1), & \alpha = 1-6\end{cases} \tag{10}$$

and

$$w_\alpha = \frac{1}{8}\begin{cases}2, & \alpha = 0\\ 1, & \alpha = 1-6\end{cases} \tag{11}$$

and the dimensionless distribution function Γ_α now becomes

$$\Gamma_\alpha = w_\alpha\left[1 + \frac{\mathbf{e}_\alpha \cdot \mathbf{u}}{c_s^2}\right]. \tag{12}$$

The speed of sound in Eqs. (5), (6), and (12) is $c_s = c/2$ for the D3Q7 lattice.

In order to calculate the normal to the interface in Eq. (2), we can use first-order central moments [14]

$$\mathbf{m}_c = \frac{1}{c}\sum_\alpha h_\alpha(\mathbf{e}_\alpha - \mathbf{u}) \tag{13}$$

to find the interface normal according to

$$\mathbf{n} = \frac{-\mathbf{m}_c}{|\mathbf{m}_c| + \epsilon} \tag{14}$$

where $\epsilon = 10^{-12}$ is a small number added to avoid division by zero in the algorithm. Alternatively, we can use finite differences to calculate the derivatives in Eq. (2). Here, we implement the following isotropic FD scheme:

$$\nabla\phi = \frac{c}{2c_s^2\,\delta x}\sum_\alpha \mathbf{e}_\alpha w_\alpha\left[\phi(\mathbf{x} + \mathbf{e}_\alpha\delta t) - \phi(\mathbf{x} - \mathbf{e}_\alpha\delta t)\right]. \tag{15}$$

Please cite this article in press as: A. Fakhari, et al., A simple phase-field model for interface tracking in three dimensions, Computers and Mathematics with Applications (2016), http://dx.doi.org/10.1016/j.camwa.2016.08.021

Table 1
L^2-norm of the error based on Eq. (17) for different case studies.

Benchmark:	Slotted sphere	Vortex	Deformation	Shear
MB-LBM (D3Q15)	0.497E−05	0.491E−05	0.267E−05	0.918E−05
FD-LBM (D3Q15)	0.498E−05	0.745E−06	0.175E−05	0.767E−06
MB-LBM (D3Q7)	0.515E−05	0.652E−05	0.458E−05	0.110E−04
FD-LBM (D3Q7)	0.507E−05	0.769E−06	0.181E−05	0.959E−06

The phase field is updated by taking the zeroth moment of the distribution function after the streaming step

$$\phi(\mathbf{x},\ t) = \sum_{\alpha} h_{\alpha}(\mathbf{x},\ t). \tag{16}$$

3. Numerical validation

We consider four different benchmarks with distinct, but prescribed, velocity fields to assess the numerical model. In each of the four cases the flows that are prescribed are such that at certain periodic intervals the phase field must return to its initial condition, meaning that the robustness of the numerical model can be tested by comparing the predicted phase field at that time to the initially prescribed field. In all of these tests, the input parameters in lattice units are $U_0 = 0.01$, $M = 0.001$, and $\xi = 3$. The number of lattice nodes in each direction of the domain is $L_0 = 256$. Errors in our simulations will be calculated using an L^2-norm as

$$\|\delta\phi\|_2 = \frac{\sqrt{\sum_{\mathbf{x}} \left[\phi(\mathbf{x},\ t_f) - \phi(\mathbf{x},\ 0)\right]^2}}{L_0^3} \tag{17}$$

where $t_f = t\,L_0/U_0$ is the final time. In what follows, we use L_0 to nondimensionalize the spatial coordinates (for example, $x^* = x/L_0$) and the radius of the spherical interface ($r^* = r/L0$). Time is also made dimensionless with the final time ($t^* = t/t_f$). For simplicity, from here on we drop the asterisks and use x, r, and t instead of x^*, r^*, and t^*, respectively.

In the numerical simulations presented in the following sections, qualitative and quantitative comparisons are made between (a) the MB-LBM on D3Q15 lattice, in which the normal to the interface is calculated by Eq. (14), (b) the FD-LBM on D3Q15 lattice, in which Eq. (15) is used to calculate the normal to the interface, (c) the MB-LBM on D3Q7 lattice, and (d) the FD-LBM on D3Q7 lattice.

3.1. Rotation of a slotted sphere

One of the most popular benchmark tests for validation of interface tracking schemes is *Zalesak's disk* [29]. For 2D flows, a slotted circle is placed in a rotational flow field [29–32]. Here, this 2D disk is replaced with a spherical interface for 3D simulations [32]. We then consider the evolution of a slotted sphere in a rotational velocity field given by

$$\begin{cases} u_x(x, y, z) = 2\pi U_0\,(0.5 - y) \\ u_y(x, y, z) = 2\pi U_0\,(x - 0.5) \\ u_z(x, y, z) = 0. \end{cases} \tag{18}$$

The magnitude of the rotational field ($2\pi U_0$) is chosen specifically such that the spherical interface revolves once after a single cycle (*i.e.*, over a time period $t = 1$).

We place a slotted sphere with the radius $r = 0.15$ at $(0.5,\ 0.75,\ 0.5)$ in a cubic domain $\in\ (1,\ 1,\ 1)$. The width of the slot (in x-direction) is 0.1 and its height (in y-direction) is $r + 0.05$ (see Fig. 1). The phase field is initialized to be one inside and zero outside the spherical interface. It is worth noting that the velocity field for this problem is not periodic. For this test problem we use zero gradient boundary conditions on all boundaries. While many previous studies have imposed periodic conditions [14,22,23,25], this gives rise to numerical artifacts originating from the corners [22,25], particularly for large Péclet numbers. Imposing zero gradient at the boundary removes this, improving the accuracy of the scheme as well as numerical stability for low mobility cases.

The final shape of the slotted sphere at $t = 1$ is shown in Fig. 2 for both moment-based and FD-based interface tracking LB models on the D3Q15 lattice as well as on the D3Q7 lattice. Visually it is apparent that the MB-LBM yields reasonable results but the FD-LBM gives a smoother profile with less oscillations on the interface. Comparing the simulations using the D3Q7 and D3Q15 lattices, we observe that the D3Q15 lattice results in a smoother interface as expected. For this problem there is a very rapid jump in the phase field across the spherical interface at initial time. This might contribute to the lower performance of the MB-LBM. A comparison of the L^2-norm of the errors in Table 1 suggests that the errors for all methods are nearly identical.

Please cite this article in press as: A. Fakhari, et al., A simple phase-field model for interface tracking in three dimensions, Computers and Mathematics with Applications (2016), http://dx.doi.org/10.1016/j.camwa.2016.08.021

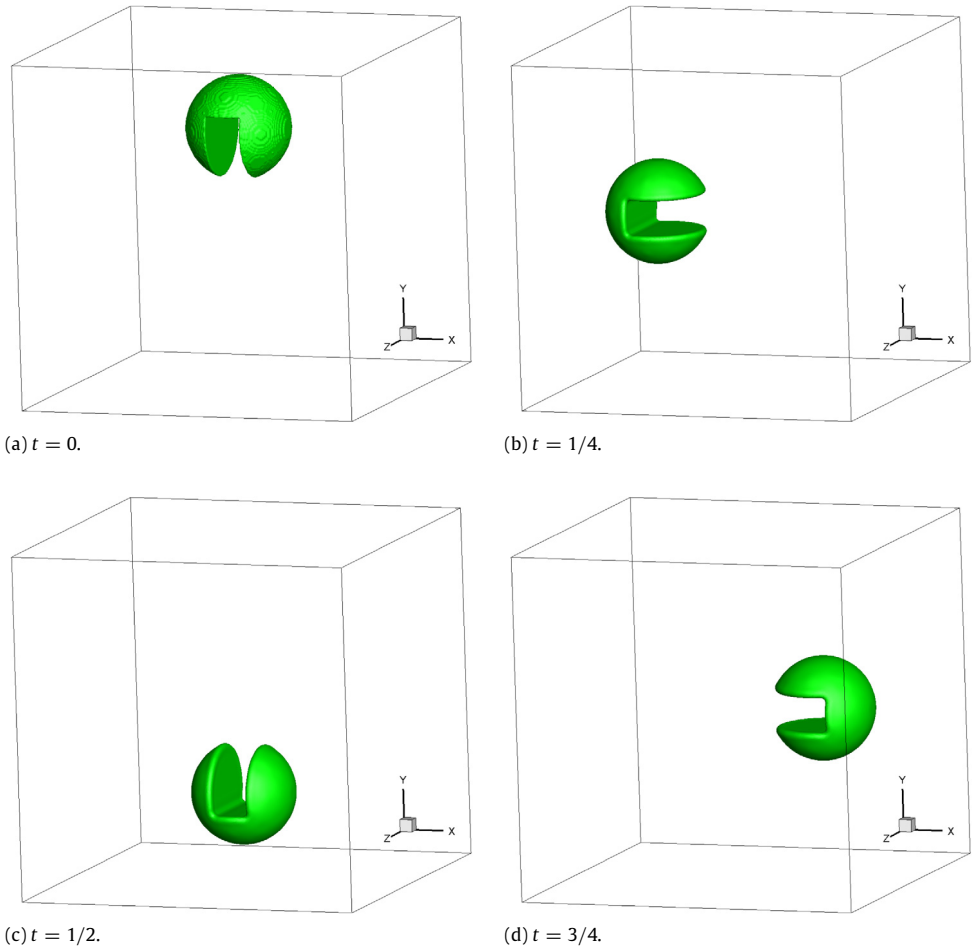

(a) $t = 0$. (b) $t = 1/4$.

(c) $t = 1/2$. (d) $t = 3/4$.

Fig. 1. Rotation of a slotted sphere with time. The isosurface of $\phi = 0.5$ is plotted.

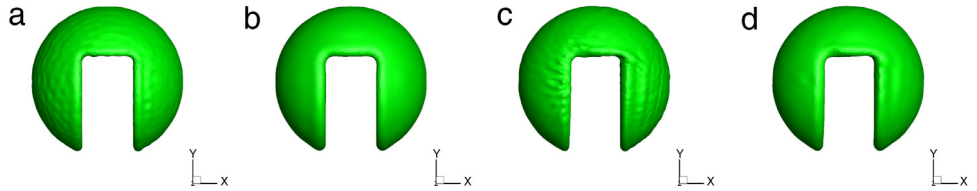

Fig. 2. Final shape of the slotted sphere at $t = 1$. The simulation results of the conservative phase-field LBM based on (a) central moments (Eq. (14)) on D3Q15, (b) finite-differences (Eq. (15)) on D3Q15, (c) central moments (Eq. (14)) on D3Q7, and (d) finite-differences (Eq. (15)) on D3Q7. The isosurface of $\phi = 0.5$ is plotted.

3.2. Vortex flow

For the second benchmark, we place a spherical interface with radius $r = 0.15$ centered at $(0.35,\ 0.35,\ 0.35)$ in a periodic domain $\in (1,\ 1,\ 1)$. The following vortex flow is prescribed [30,32]:

$$\begin{cases} u_x(x, y, z) = 2U_0 \sin^2(\pi x) \sin(2\pi y) \sin(2\pi z) \cos(\pi t) \\ u_y(x, y, z) = -U_0 \sin^2(\pi y) \sin(2\pi z) \sin(2\pi x) \cos(\pi t) \\ u_z(x, y, z) = -U_0 \sin^2(\pi z) \sin(2\pi x) \sin(2\pi y) \cos(\pi t). \end{cases} \tag{19}$$

The $\cos(\pi t)$ term in the velocity field makes the flow reversible such that the interface starts reverting at $t = 1$ and fully recovers its initial shape at $t = 2$. For this vortex flow, the phase field is initialized according to Eq. (3).

The evolution of the interface at different times is shown in Fig. 3. The side-by-side comparison between the MB-LBM and the FD-LBM on both D3Q15 and D3Q7 lattices at $t = 2$, when the original interface should be recovered, is shown in Fig. 4.

Please cite this article in press as: A. Fakhari, et al., A simple phase-field model for interface tracking in three dimensions, Computers and Mathematics with Applications (2016), http://dx.doi.org/10.1016/j.camwa.2016.08.021

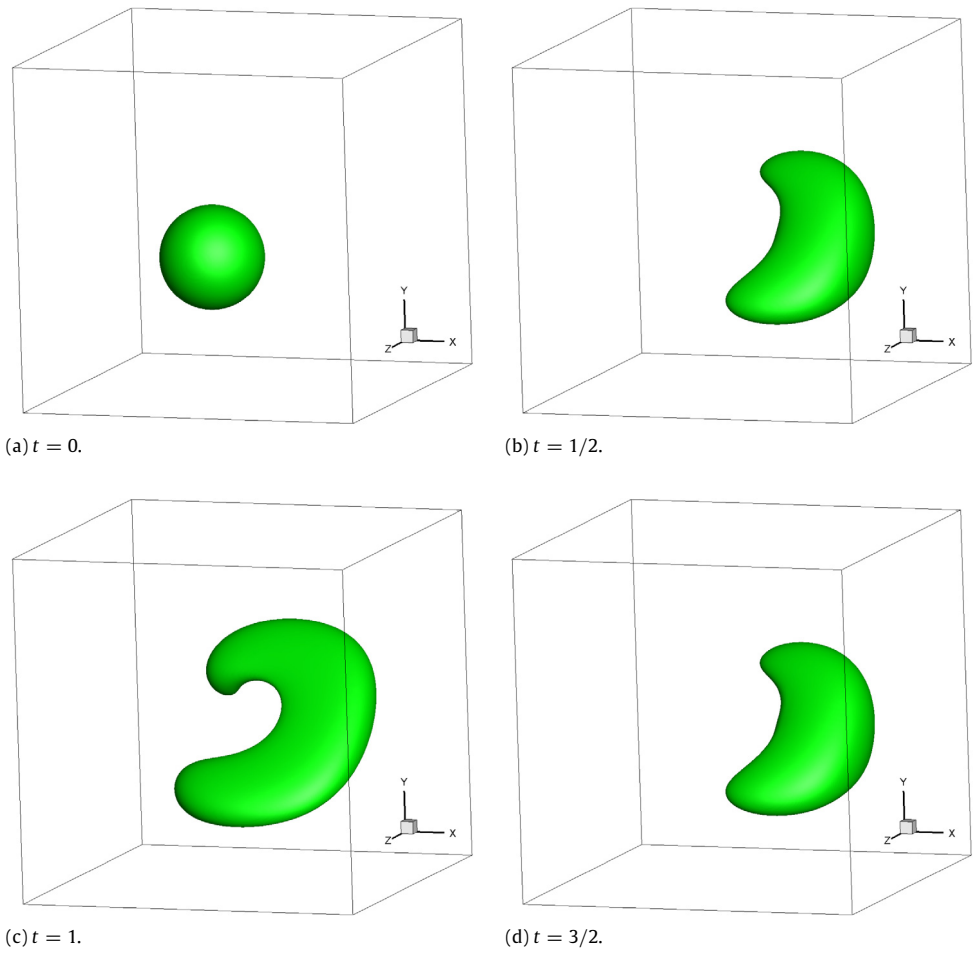

(a) $t = 0$. (b) $t = 1/2$.

(c) $t = 1$. (d) $t = 3/2$.

Fig. 3. Evolution of a spherical interface under vortex flow. The isosurface of $\phi = 0.5$ is plotted.

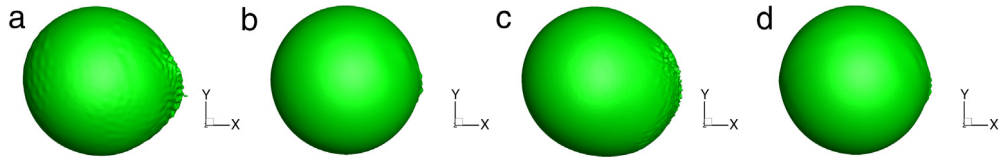

Fig. 4. Final shape of the spherical interface in a vortex flow at $t = 2$. The simulation results of the CPF-LBM based on (a) MB-LBM on D3Q15, (b) FD-LBM on D3Q15, (c) MB-LBM on D3Q7, and (d) FD-LBM on D3Q7. The isosurface of $\phi = 0.5$ is plotted.

Visually it is apparent that the MB-LBM suffers from unwanted wiggles at the interface, similar to the previous benchmark. As previously described [14], the moment-based approach seems to be susceptible to grid-scale oscillations. Increasing the interfacial thickness ξ can help damp these. It is also apparent that the FD-based model yields smoother results and a more accurate solution. As noted in Table 1, the calculated error for the FD-based model is an order of magnitude smaller than the moment-based approach. Comparing the D3Q15 and D3Q7 lattices, it is also evident that the D3Q15 lattice gives us more accurate results. Although visually the interface obtained by the MB-LBM on D3Q7 lattice seems to be smoother than the D3Q15 counterpart in Fig. 4, note that overall the quantitative error, as measured in Table 1, is smaller for the D3Q15 lattice, as expected.

3.3. Deformation field

Next we employ a more complex velocity field which induces more stretching and deformation than the previous two cases. Again, we place a spherical interface with radius $r = 0.2$ at $(0.5,\ 0.5,\ 0.5)$ in a periodic domain $\in (1,\ 1,\ 1)$. The

Please cite this article in press as: A. Fakhari, et al., A simple phase-field model for interface tracking in three dimensions, Computers and Mathematics with Applications (2016), http://dx.doi.org/10.1016/j.camwa.2016.08.021

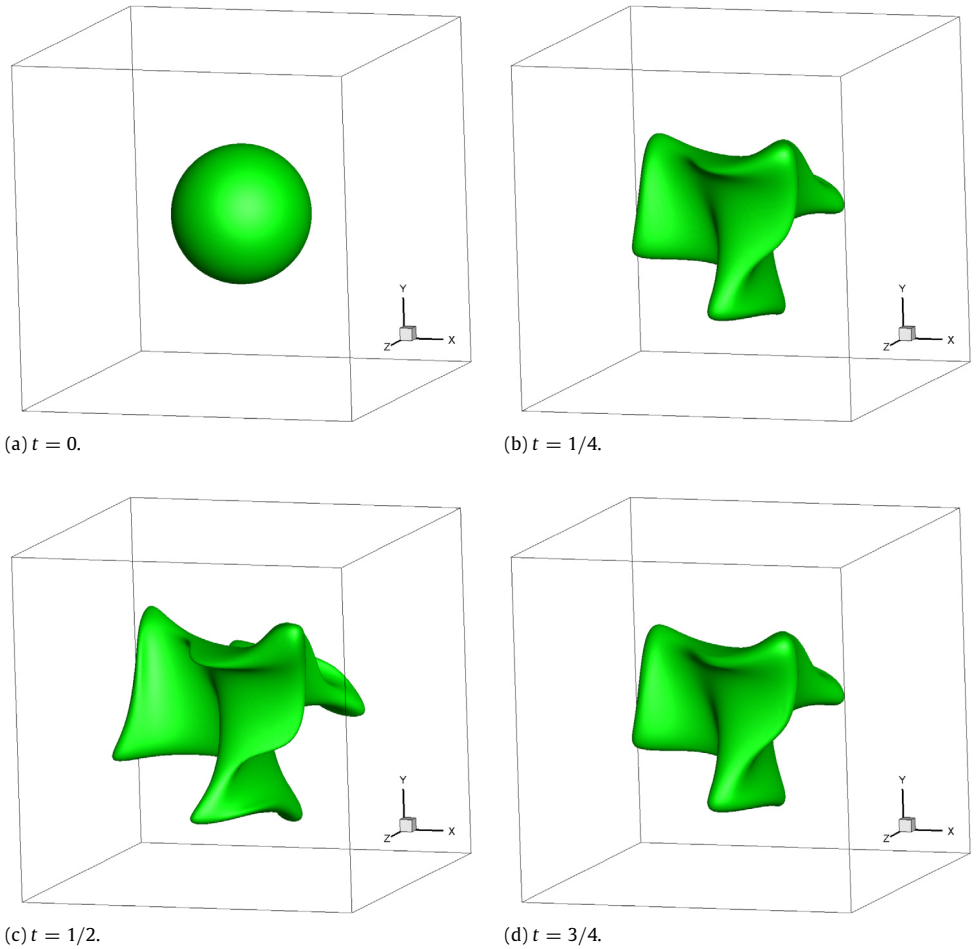

(a) $t = 0$. (b) $t = 1/4$.

(c) $t = 1/2$. (d) $t = 3/4$.

Fig. 5. Evolution of a spherical interface under swirling deformation. The isosurface of $\phi = 0.5$ is plotted.

following flow field is imposed [33]:

$$\begin{cases} u_x(x,y,z) = \dfrac{U_0}{2}[\sin(4\pi(x-0.5))\sin(4\pi(y-0.5)) + \cos(4\pi(z-0.5))\cos(4\pi(x-0.5))]\cos(\pi t) \\ u_y(x,y,z) = \dfrac{U_0}{2}[\sin(4\pi(y-0.5))\sin(4\pi(z-0.5)) + \cos(4\pi(x-0.5))\cos(4\pi(y-0.5))]\cos(\pi t) \\ u_z(x,y,z) = \dfrac{U_0}{2}[\sin(4\pi(z-0.5))\sin(4\pi(x-0.5)) + \cos(4\pi(y-0.5))\cos(4\pi(z-0.5))]\cos(\pi t). \end{cases} \tag{20}$$

Again the $\cos(\pi t)$ term causes the interface to return to its original position at $t = 1$. As in the previous test, the phase-field profile is initially smoothly defined by Eq. (3).

This flow has multiple vortices within the computational domain, resulting in a more chaotic deformation of the interface (Fig. 5). At $t = 1$ the interface reverts to its initial position as shown in Fig. 6. While the general shape is well recovered, there is a clear generation of some kinks on the interface for both formulations. These kinks are more pronounced for the MB-LBM, suggesting a larger numerical error relative to the FD-LBM, which matches quantitative measures in Table 1.

3.4. Shear flow

For our final benchmark, we place a spherical interface with radius $r = 0.2$ at $(0.3, 0.3, 0.5)$ in a cubic domain $\in (1, 1, 1)$. We extend the 2D shear flow employed by Rudman [31] to 3D such that

$$\begin{cases} u_x(x,y,z) = \pi\, U_0 \cos(\pi(x-0.5))\,[\sin(\pi(z-0.5)) - \sin(\pi(y-0.5))]\cos(\pi t) \\ u_y(x,y,z) = \pi\, U_0 \cos(\pi(y-0.5))\,[\sin(\pi(x-0.5)) - \sin(\pi(z-0.5))]\cos(\pi t) \\ u_z(x,y,z) = \pi\, U_0 \cos(\pi(z-0.5))\,[\sin(\pi(y-0.5)) - \sin(\pi(x-0.5))]\cos(\pi t). \end{cases} \tag{21}$$

Please cite this article in press as: A. Fakhari, et al., A simple phase-field model for interface tracking in three dimensions, Computers and Mathematics with Applications (2016), http://dx.doi.org/10.1016/j.camwa.2016.08.021

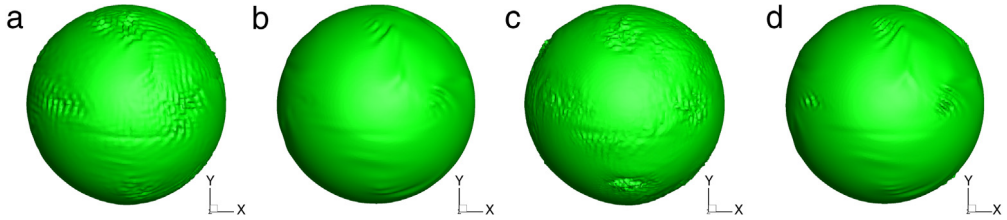

Fig. 6. Final shape of the spherical interface in a severe deformation field at $t = 1$. The simulation results of the CPF-LBM based on (a) MB-LBM on D3Q15, (b) FD-LBM on D3Q15, (c) MB-LBM on D3Q7, and (d) FD-LBM on D3Q7. The isosurface of $\phi = 0.5$ is plotted.

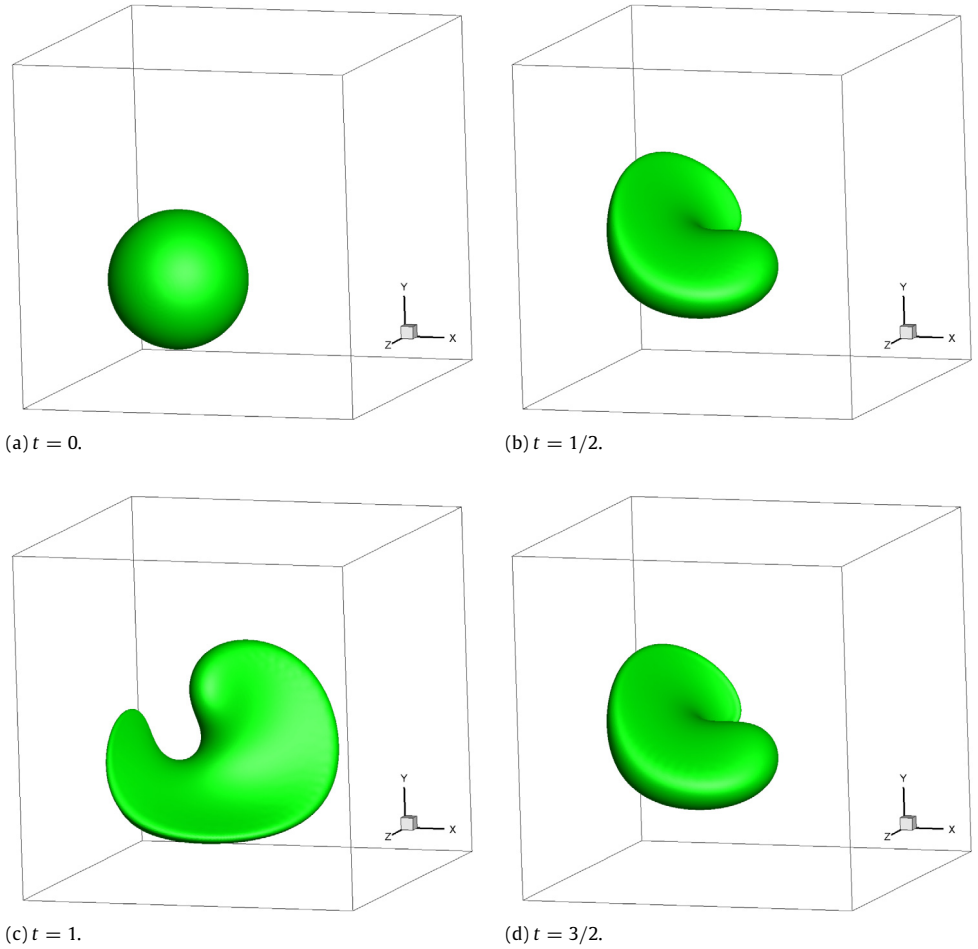

(a) $t = 0$. (b) $t = 1/2$.

(c) $t = 1$. (d) $t = 3/2$.

Fig. 7. Evolution of a spherical interface under shear flow. The isosurface of $\phi = 0.5$ is shown.

The phase field is initialized according to Eq. (3), and, similar to the slotted sphere case, zero-gradient BCs are used in all directions. For this velocity field, the interface will return to its original position at $t = 2$.

The evolution of the interface with time is illustrated in Fig. 7. The topological changes in Fig. 7 are seemingly not as extreme as in the previous benchmark, but flows like these can cause more distortion as is evident from Fig. 8. In addition to numerical wiggles on the interface, as seen before, the original spherical shape is not as cleanly recovered and appears more distorted. The manifestation of this noticeable distortion is evident in Table 1. Note that the error of the FD-LBM (for both D3Q15 and D3Q7 lattices) is an order of magnitude smaller than the MB-LBM. While this is clearly an improvement, we must keep in mind that this increased accuracy using the FD-LBM comes at a cost, requiring a non-local collision step, which the moment-based approach does not.

On the other hand, comparing the CPF-LBM on D3Q15 and D3Q7 lattices in Table 1, we note that the D3Q15 lattice results in slightly more accurate solutions. The computations on the D3Q7 lattice, however, are almost twice as fast as those on the D3Q15 lattice. This could be beneficial for massively parallel (or serial) computations where very high accuracy is not desired.

Please cite this article in press as: A. Fakhari, et al., A simple phase-field model for interface tracking in three dimensions, Computers and Mathematics with Applications (2016), http://dx.doi.org/10.1016/j.camwa.2016.08.021

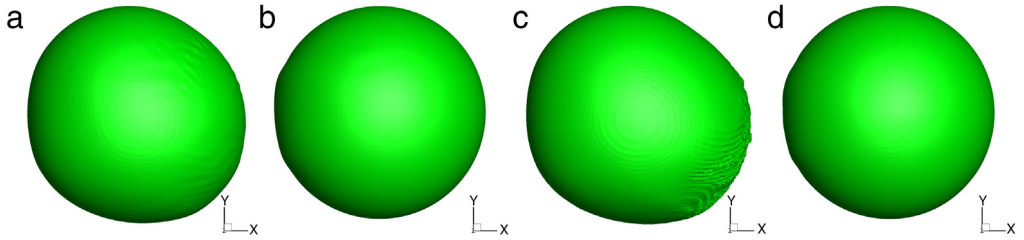

Fig. 8. Final shape of the spherical interface at $t = 2$. The simulation results of the conservative phase-field LBE based on (a) MB-LBM on D3Q15, (b) FD-LBM on D3Q15, (c) MB-LBM on D3Q7, and (d) FD-LBM on D3Q7. The isosurface of $\phi = 0.5$ is shown.

3.5. Discussion of the benchmark results

Table 1 highlights that the D3Q15 lattice outperforms the D3Q7 lattice in terms of accuracy. The reason for this becomes clear when considering the equivalent partial differential equations for the LBM, as can be obtained by asymptotic analysis (see for example [34,35] and Appendix G in [28]). Recall that the phase indicator $\phi(\mathbf{x}, t)$ is the zeroth moment of the phase-field distribution function $h_\alpha(\mathbf{x}, t)$. Asymptotic analysis [14] reveals that the corresponding flux density of the phase indicator is given by the first-order moments of the distribution $h_\alpha(\mathbf{x}, t)$. Second-order moments are again flux densities of the first-order moments and so on. In the case of the phase-field equation it is sufficient for a model to cover zeroth- and first-order moments, that is the phase indicator and its flux density. Higher-order moments contribute only to the numerical error of the method and their influence is diminished by refining the grid and the time step. For a second-order-accurate advection–diffusion equation, moments of order two and higher are formally irrelevant. Due to its limited degrees of freedom the D3Q7 lattice offers only three of the six second-order moments as independent observable quantities. Being designed for solving the hydrodynamic equations, which require more isotropy than the phase-field equation, the D3Q15 lattice has all six second-order moments as independent observable quantities. This means it offers enough degrees of freedom to also adjust the flux densities of the first-order moments. Hence, the leading numerical errors in the phase-field equation can be eliminated. It is important to note that this does not happen automatically but requires a careful choice of the second-order moments. As for the phase indicator itself there are two major components of the fluxes of any moment: the advective flux and the diffusive flux. The advective flux is responsible for Galilean invariance. For the second-order moments Galilean invariance is imposed by adding all second-order monomials in velocity to the equilibrium function. This cannot be done on the D3Q7 lattice and Galilean invariance is hence violated (the diffusion coefficient is found to be a function of velocity). The advective flux is governed by the relaxation rate of the respective moment. Adjusting this independently would require a multi relaxation time approach. If the equivalent partial differential equation at the leading order of the error is carefully tailored such that its solution is null, the order of convergence of the method increases. However, in addition to the fluxes of higher order there is an influence of initial and boundary conditions and of the external velocity field on the leading order error. It is therefore difficult to obtain a genuine higher order method. It is observed here that even though the method using more speeds is not of higher order, it still eliminates enough numerical artifacts that it results in an appreciable improvement of the overall results.

3.6. Efficiency

A comparison between the run-time of D3Q7 and D3Q15 lattices is shown in Table 2 for both MB-LBM and FD-LBM. An OpenMP Parallel Fortran code is executed using the Intel compiler on a personal computer with Intel® Core™ i7-4910MQ processor (CPU) @2.90 GHz base frequency and 32.0 GB shared memory (RAM). The results in Table 2 show the computation cost per time step on a $256 \times 256 \times 256$ grid. As can be seen, the computations using the D3Q7 lattice, although less accurate, are roughly performed twice as fast as those using the D3Q15 lattice, whether FD-LBM or MB-LBM is utilized. This is expected since the D3Q15 lattice has approximately twice the number of microscopic velocities (15) as the D3Q7 lattice (7). Comparing MB-LBM and FD-LBM on the same lattice, we see that the finite-difference-based model, although non-local, is competitive compared with the moment-based model. Note that these results are obtained on a shared-memory machine. Given that the MB-LBM is entirely local, this behavior would change dramatically in favor of the MB-LBM on distributed-memory machines using, say, MPI parallel programming. It should be noted that the current results are obtained using a modular code that strives for generality and readability rather than efficiency and optimization. As such, the results presented in Table 2 should not be taken as decisive as to the actual performance of the methods, but should rather be considered as a comparative guideline.

4. Three-phase contact line

In all the previous benchmarks we only considered the evolution of an interface due to a given velocity field in a domain with either periodic or zero-gradient BCs with no solid boundaries. Fluid–solid interactions, however, are important across a

Please cite this article in press as: A. Fakhari, et al., A simple phase-field model for interface tracking in three dimensions, Computers and Mathematics with Applications (2016), http://dx.doi.org/10.1016/j.camwa.2016.08.021

Table 2
Comparison between the performance of MB-LBM and FD-LBM on D3Q7 and D3Q15 lattices. The CPU time (in seconds) per iteration for a 256^3 grid on a shared-memory PC using 4 processors.

	D3Q15 (MB)	D3Q15 (FD)	D3Q7 (MB)	D3Q7 (FD)
CPU time (s)	1.230	1.289	0.595	0.668

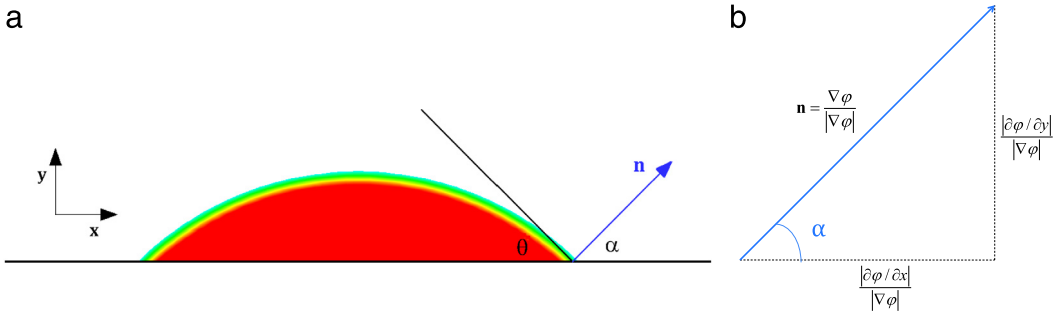

Fig. 9. A schematic of the three-phase contact angle. θ is the contact angle and $\alpha = \pi/2 - \theta$ is the angle between the interface normal and the horizontal wall (2D projection of the interface normal is shown).

broad spectrum of scientific and engineering applications, such as multiphase flow and transport through porous media [18] and binary fluid interaction with hydrophobic nanochannels [36,37].

In this section we propose a simple and accurate remedy for the conservative phase-field equation to model a three-phase contact line. We impose the contact angle between a two-phase (liquid–gas) flow and the third phase (solid) using a simple mathematical formula. The same relations also hold for the contact angle between a binary fluid (liquid–liquid or gas–gas) and a solid surface. For brevity, numerical simulations will be performed using the FD-LBM on the D3Q15 lattice. Although the chosen model appears to be the most accurate of considered methods, a similar approach is possible using the other models and/or lattices.

For the sake of simplicity, let us assume a solid wall is aligned with the horizontal axis in the x-direction; note the model can be generalized to arbitrarily-oriented solid surfaces. Referring to Fig. 9, the contact angle θ between a semispherical interface and a flat wall can be written as $\theta = \pi/2 - \alpha$, where α is the angle between the unit vector normal to the interface and the flat substrate. Noting that the projection of the interface normal on the x–z plane is proportional to $\sqrt{(\partial\phi/\partial x)^2 + (\partial\phi/\partial z)^2}$, the following mathematical formula holds at the surface of the solid wall:

$$\tan\alpha = \frac{-\partial\phi/\partial y}{\sqrt{(\partial\phi/\partial x)^2 + (\partial\phi/\partial z)^2}} \tag{22}$$

which gives us

$$\frac{\partial\phi}{\partial y} = -\sqrt{\left(\frac{\partial\phi}{\partial x}\right)^2 + \left(\frac{\partial\phi}{\partial z}\right)^2}\,\tan\alpha. \tag{23}$$

In contrast to free-energy-based formulas for contact line treatment, the above relationship is very simple and straightforward to implement. Derivatives of the phase field along the x- and z-directions are readily calculated using central differences, and the derivative of the phase field in the normal (y) direction gives us the unknown data. For the half-way (link) bounce-back boundary condition, which is implemented in this study, Eq. (23) at the bottom wall becomes:

$$\phi_{i,0,k} = \phi_{i,1,k} + \frac{\delta x}{2}\sqrt{\left(\phi_{i+1,1,k} - \phi_{i+1,1,k}\right)^2 + \left(\phi_{i,1,k+1} - \phi_{i,1,k-1}\right)^2}\,\tan\alpha \tag{24}$$

where i and k denote discretized lattice indices in the x- and z-directions, respectively. The lattice node with $j = 0$ indicates the exterior (ghost cell) layer, and the effective location of the solid wall is half-way between $j = 0$ and $j = 1$. Although, as described in Ref. [14], we might be able to use moments in calculation of the gradients, we advocate finite differences for reasons of numerical stability and accuracy in addition to clarity of the algorithm.

Here we present two test cases with different contact angles: (1) a hydrophilic surface with $\theta = 45^\circ$, and (2) a hydrophobic surface with $\theta = 135^\circ$. Initially, we place a semi-spherical (semi-circular in 2D) droplet with $r = 0.125$ at $(0.5,\ 0,\ 0.5)$ in a computational domain of size $(1,\ 0.5,\ 1)$. 128 lattice points in the x- and z-directions and 64 lattice points in the y-direction are used. For 2D simulations $\partial\phi/\partial z$ is set to zero in the above formulas. The boundary conditions are periodic in x- and z-directions and no-slip at the top and bottom of the domain, where bounce-back on the link is used to find the values of the distribution function. The interface is tracked by solving Eq. (4) and using Eq. (24) to find the unknown

Please cite this article in press as: A. Fakhari, et al., A simple phase-field model for interface tracking in three dimensions, Computers and Mathematics with Applications (2016), http://dx.doi.org/10.1016/j.camwa.2016.08.021

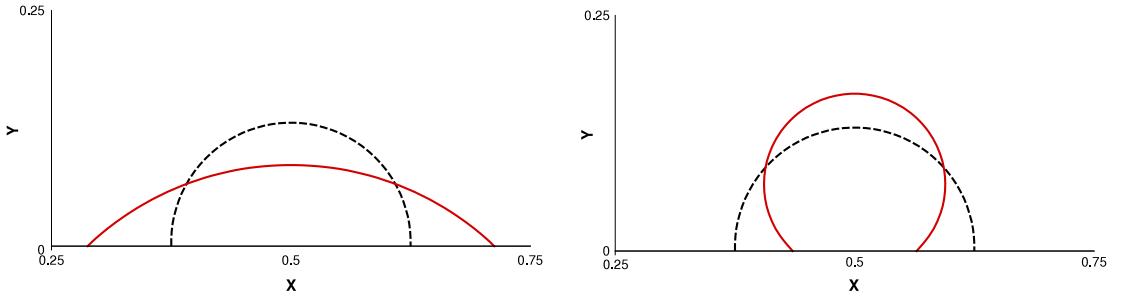

(a) $\theta = 45^\circ$. (b) $\theta = 135^\circ$.

Fig. 10. Three-phase contact line in 2D. Initial profile (black dashed line) and equilibrium profile (solid red line) for two different contact angles: (a) $\theta = 45^\circ$, (b) $\theta = 135^\circ$.

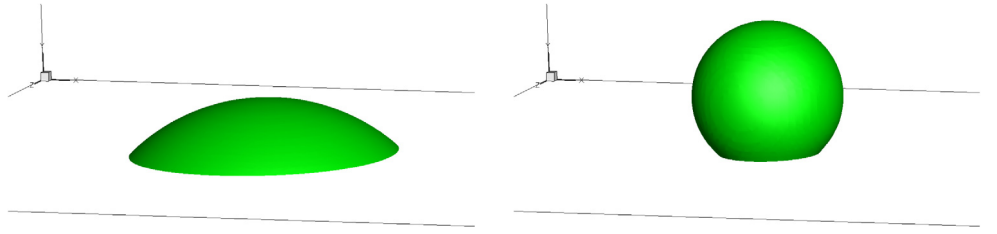

(a) $\theta = 45^\circ$. (b) $\theta = 135^\circ$.

Fig. 11. Three-phase contact line in 3D. Isosurface of $\phi = 0.5$ for two contact angles: (a) $\theta = 45^\circ$, (b) $\theta = 135^\circ$.

phase-field values, which are needed in calculation of the normal to the interface in Eq. (15). The hydrodynamic properties (density, velocity, and pressure) are found by using the LBM proposed in Ref. [38]. For the following examples, the density and viscosity ratios are both set to 10.

Fig. 10 shows the results of the 2D simulations. The initial profile is shown by a black dashed line and the final shape of the interface after 10 000 iterations is shown by the solid red line. Similarly, 3D simulations are shown in Fig. 11. The isosurface of $\phi = 0.5$ for the drop sitting on both hydrophobic and hydrophilic surfaces is shown. As can be seen, the proposed formula is successful in modeling the contact angle between a fluid–fluid–solid interface.

5. Summary

A three-dimensional conservative LBE for tracking the interface between different fluids was developed in this study. In this model, the only gradient that must be explicitly calculated is that of the normal to the interface, which is a first-order derivative. An entirely local collision step was devised, based on central moments, to obtain this first-order derivative. This was achieved by taking the first central moment of the phase-field distribution function. Alternatively, finite-differences were used to calculate the interface normal. The choice between the first central moment and FD scheme is made by compromising between the locality and the accuracy of the numerical scheme. The moment-based approach, while very simple and efficient for parallel computing, appears to suffer from grid-scale oscillations. This is mainly due to approximating the interface normal from the first-order moments. Although this caveat does not make the scheme numerically unstable, it reduces the fidelity of the simulations compared with the FD-based approach. Complete elimination of these unwanted grid-scale oscillations merits future study.

Appendix. Weight coefficients and microscopic velocity sets for D3Q19 and D3Q27

The discrete velocity set for the D3Q19 lattice is

$$\mathbf{e}_\alpha = c \begin{cases} (0,\ 0,\ 0), & \alpha = 0 \\ (\pm 1,\ 0,\ 0), (0,\ \pm 1,\ 0), (0,\ 0,\ \pm 1), & \alpha = 1 - 6 \\ (\pm 1,\ \pm 1,\ 0), (\pm 1,\ 0,\ \pm 1), (0,\ \pm 1,\ \pm 1), & \alpha = 7 - 18 \end{cases} \tag{A.1}$$

and the weight coefficients are

$$w_\alpha = \frac{1}{36} \begin{cases} 12, & \alpha = 0 \\ 2, & \alpha = 1 - 6 \\ 1, & \alpha = 7 - 18. \end{cases} \tag{A.2}$$

Please cite this article in press as: A. Fakhari, et al., A simple phase-field model for interface tracking in three dimensions, Computers and Mathematics with Applications (2016), http://dx.doi.org/10.1016/j.camwa.2016.08.021

The discrete velocity set for the D3Q27 lattice is

$$\mathbf{e}_\alpha = c \begin{cases} (0,\ 0,\ 0), & \alpha = 0 \\ (\pm 1,\ 0,\ 0),\ (0,\ \pm 1,\ 0),\ (0,\ 0,\ \pm 1), & \alpha = 1 - 6 \\ (\pm 1,\ \pm 1,\ 0),\ (\pm 1,\ 0,\ \pm 1),\ (0,\ \pm 1,\ \pm 1), & \alpha = 7 - 18 \\ (\pm 1,\ \pm 1,\ \pm 1), & \alpha = 19 - 26 \end{cases} \tag{A.3}$$

and the corresponding weight coefficients are

$$w_\alpha = \frac{1}{216} \begin{cases} 64, & \alpha = 0 \\ 16, & \alpha = 1 - 6 \\ 4, & \alpha = 7 - 18 \\ 1, & \alpha = 19 - 26. \end{cases} \tag{A.4}$$

The lattice speed of sound for all D3Q15, D3Q19, and D3Q27 lattices is $c_s = c/\sqrt{3}$.

References

[1] G. Tryggvason, R. Scardovelli, S. Zaleski, Direct Numerical Simulations of Gas–Liquid Multiphase Flows, Cambridge University Press, 2011.
[2] C. Hirt, B. Nichols, Volume of fluid (VOF) method for the dynamics of free boundaries, J. Comput. Phys. 39 (1981) 201–225.
[3] J. Glimm, J. Grove, B. Lindquist, O. McBryan, G. Tryggvason, The bifurcation of tracked scalar waves, SIAM J. Sci. Stat. Comput. 9 (1988) 61.
[4] S.O. Unverdi, G. Tryggvason, A front-tracking method for viscous, incompressible, multi-fluid flows, J. Comput. Phys. 100 (1992) 25–37.
[5] S. Osher, J.A. Sethian, Fronts propagating with curvature dependent speed: Algorithms based on Hamilton-Jacobi formulations, J. Comput. Phys. 79 (1988) 12–49.
[6] E. Olsson, G. Kreiss, A conservative level set method for two phase flow, J. Comput. Phys. 210 (2005) 225–246.
[7] J.S. Rowlinson, B. Widom, Molecular Theory of Capillarity, Clarendon Press, Oxford, 1989.
[8] D. Jacqmin, Calculation of two-phase Navier-Stokes flows using phase-field modeling, J. Comput. Phys. 155 (1999) 96.
[9] J.W. Cahn, J.E. Hilliard, Free energy of a nonuniform system. i. interfacial free energy, J. Chem. Phys. 28 (1958) 258.
[10] S.M. Allen, J.W. Cahn, Mechanisms of phase transformations within the miscibility gap of Fe-Rich Fe-Al alloys, Acta Metall. 24 (1976) 425.
[11] Y. Sun, C. Beckermann, Sharp interface tracking using the phase-field equation, J. Comput. Phys. 220 (2007) 626–653.
[12] P.-H. Chiu, Y.-T. Lin, A conservative phase field method for solving incompressible two-phase flows, J. Comput. Phys. 230 (2011) 185–204.
[13] A. Fakhari, M.H. Rahimian, Phase-field modeling by the method of lattice Boltzmann equations, Phys. Rev. E 81 (2010) 036707.
[14] M. Geier, A. Fakhari, T. Lee, Conservative phase-field lattice Boltzmann model for interface tracking equation, Phys. Rev. E 91 (2015) 063309.
[15] A. Cali, S. Succi, A. Cancelliere, R. Benzi, M. Gramignani, Diffusion and hydrodynamic dispersion with the lattice Boltzmann method, Phys. Rev. A 45 (1992) 5771.
[16] B. Shi, Z. Guo, Lattice Boltzmann model for nonlinear convection-diffusion equations, Phys. Rev. E 79 (2009) 016701.
[17] D. Yu, R. Mei, L.-S. Luo, W. Shyy, Viscous flow computations with the method of lattice Boltzmann equation, Prog. Aerosp. Sci. 39 (2003) 329.
[18] H. Huang, M.C. Sukop, X.-Y. Lu, Multiphase Lattice Boltzmann Methods: Theory and Application, Wiley-Blackwell, 2015.
[19] X. He, L.-S. Luo, Theory of the lattice Boltzmann method: From the Boltzmann equation to the lattice Boltzmann equation, Phys. Rev. E 56 (1997) 6811.
[20] T.J. Spencer, I. Halliday, C.M. Care, A local lattice Boltzmann method for multiple immiscible fluids and dense suspensions of drops, Phil. Trans. R. Soc. A 369 (2011) 2255–2263.
[21] J. Tölke, G.D. Prisco, Y. Mu, A lattice Boltzmann method for immiscible two-phase Stokes flow with a local collision operator, Comput. Math. Appl. 65 (2013) 864–881.
[22] H.W. Zheng, C. Shu, Y.T. Chew, Lattice Boltzmann interface capturing method for incompressible flows, Phys. Rev. E 72 (2005) 056705.
[23] Y.Q. Zu, S. He, Phase-field-based lattice Boltzmann model for incompressible binary fluid systems with density and viscosity contrasts, Phys. Rev. E 87 (2013) 043301.
[24] A. Fakhari, T. Lee, Multiple-relaxation-time lattice Boltzmann method for immiscible fluids at high Reynolds numbers, Phys. Rev. E 87 (2013) 023304.
[25] H. Liang, B.C. Shi, Z.L. Guo, Z.H. Chai, Phase-field-based multiple-relaxation-time lattice Boltzmann model for incompressible multiphase flows, Phys. Rev. E 89 (2014) 053320.
[26] Q. Lou, Z. Guo, Interface-capturing lattice Boltzmann equation model for two-phase flows, Phys. Rev. E 91 (2015) 013302.
[27] P.G. de Gennes, Wetting: statics and dynamics, Rev. Modern Phys. 57 (1985) 827–863.
[28] M. Geier, M. Schönherr, A. Pasquali, M. Krafczyk, The cumulant lattice Boltzmann equation in three dimensions: Theory and validation, Comput. Math. Appl. 70 (2015) 507–547.
[29] S.T. Zalesak, Fully multidimensional flux-corrected transport algorithms for fluids, J. Comput. Phys. 31 (1979) 335.
[30] R. Leveque, High-resolution conservative algorithms for advection in incompressible flow, SIAM J. Numer. Anal. 33 (1996) 627–665.
[31] M. Rudman, Volume-tracking methods for interfacial flow calculations, Internat. J. Numer. Methods Fluids 24 (1997) 671–691.
[32] D. Enright, R. Fedkiw, J. Ferziger, I. Mitchell, A hybrid particle level set method for improved interface capturing, J. Comput. Phys. 183 (2002) 83–116.
[33] W.J. Rider, D.B. Kothe, Reconstructing volume tracking, J. Comput. Phys. 141 (1998) 112–152.
[34] M. Junk, A. Klar, L.-S. Luo, Asymptotic analysis of the lattice Boltzmann equation, J. Comput. Phys. 210 (2005) 676–704.
[35] F. Dubois, Equivalent partial differential equations of a lattice Boltzmann scheme, Comput. Math. Appl. 55 (2008) 1441–1449.
[36] M. Sbragaglia, R. Benzi, L. Biferale, S. Succi, F. Toschi, Surface roughness-hydrophobicity coupling in microchannel and nanochannel flows, Phys. Rev. Lett. 97 (2006) 204503.
[37] S. Chakraborty, D. Chatterjee, C. Bakli, Nonlinear amplification in electrokinetic pumping in nanochannels in the presence of hydrophobic interactions, Phys. Rev. Lett. 110 (2013) 184503.
[38] A. Fakhari, M. Geier, T. Lee, A mass-conserving lattice Boltzmann method with dynamic grid refinement for immiscible two-phase flows, J. Comput. Phys. 315 (2016) 434–457.

Please cite this article in press as: A. Fakhari, et al., A simple phase-field model for interface tracking in three dimensions, Computers and Mathematics with Applications (2016), http://dx.doi.org/10.1016/j.camwa.2016.08.021